nature COMMUNICATIONS

ARTICLE

https://doi.org/10.1038/s41467-019-11542-w OPEN

CO_2 electrochemical catalytic reduction with a highly active cobalt phthalocyanine

Min Wang[1], Kristian Torbensen[1], Danielle Salvatore[2], Shaoxuan Ren[3], Dorian Joulié[1,3], Fabienne Dumoulin[4], Daniela Mendoza[1,6], Benedikt Lassalle-Kaiser[6], Umit Işci[4], Curtis P. Berlinguette[2,3,5] & Marc Robert[1]

Molecular catalysts that combine high product selectivity and high current density for CO_2 electrochemical reduction to CO or other chemical feedstocks are urgently needed. While earth-abundant metal-based molecular electrocatalysts with high selectivity for CO_2 to CO conversion are known, they are characterized by current densities that are significantly lower than those obtained with solid-state metal materials. Here, we report that a cobalt phthalocyanine bearing a trimethyl ammonium group appended to the phthalocyanine macrocycle is capable of reducing CO_2 to CO in water with high activity over a broad pH range from 4 to 14. In a flow cell configuration operating in basic conditions, CO production occurs with excellent selectivity (ca. 95%), and good stability with a maximum partial current density of 165 mA cm^{-2} (at −0.92 V vs. RHE), matching the most active noble metal-based nanocatalysts. These results represent state-of-the-art performance for electrolytic carbon dioxide reduction by a molecular catalyst.

[1] Université de Paris, Laboratoire d'Electrochimie Moléculaire, CNRS, F-75013 Paris, France. [2] Department of Chemical and Biological Engineering, The University of British Columbia, 2360 East Mall, Vancouver, BC V6Y 1Z3, Canada. [3] Department of Chemistry, The University of British Columbia, 2036 Main Mall, Vancouver, BC V6T 1Z1, Canada. [4] Gebze Technical University, Department of Chemistry, 41400 Gebze, Kocaeli, Turkey. [5] Stewart Blusson Quantum Matter Institute, The University of British Columbia, 2355 East Mall, Vancouver, BC V6T 1Z4, Canada. [6] Synchrotron SOLEIL, L'Orme des Merisiers, Saint-Aubin, 91192 Gif-sur-Yvette, France. Correspondence and requests for materials should be addressed to U.I. (email: u.isci@gtu.edu.tr) or to C.P.B. (email: cberling@chem.ubc.ca) or to M.R. (email: robert@univ-paris-diderot.fr)

CO_2 can potentially be used as a renewable feedstock in electrochemical devices for sustainable energy storage in the form of synthetic fuels or fuel precursors (such as CO, CH_3OH, and CH_4), or for commodity chemicals. Hence, electrochemical reduction of CO_2 is an attractive way for industry to exploit surplus sustainable electricity in periods of low demand and it may contribute to mitigating the environmental impact caused by the massive release of CO_2[1–3]. However, the efficient and robust electrolytically driven reduction of CO_2 remains a formidable challenge for the scientific community. Fundamentally new approaches are needed to realize the selective transformation of CO_2 into desired products in an industrial setting.

There are several approaches available to catalyze the carbon dioxide reduction reaction (CO_2RR), including molecular catalysts[4–7]. Molecular transition metal catalysts offer the distinct advantage of allowing for the fine-tuning of the primary and secondary coordination spheres by manipulating the chelating environment and the steric and electronic effects of the ligands. The ability to improve catalytic efficiency and product selectivity through the rational optimization of the ligand structure is a feature not accessible to the solid-state catalysts common to pilot-scale electrolyzer units[8,9].

There now exist a range of known molecular catalysts, including those based on noble (e.g., Ru, Ir, and Re) and earth-abundant metals (e.g., Co, Ni, Fe, Mn, and Cu)[4–12]. These catalysts typically mediate a two electron reduction of CO_2 to either CO or formate with reasonable efficiencies, but in organic solvents. (there are also rare reports demonstrating molecules to catalyze highly reduced products such as light hydrocarbons)[13–15]. Integrating molecules with thin porous carbon films, such as carbon powder, carbon nanotubes, or graphene to form hybrid catalytic materials has proven to be a promising strategy to selectively achieve CO production in pure aqueous conditions. Importantly, these systems used earth-abundant metal catalysts such as Fe and Co porphyrins[16–23], Mn bipyridine complexes[24,25], Co quaterpyridines[26], and Co phthalocyanines[27–32]. Good performances have been obtained in close to neutral conditions (pH 7–7.5) with excellent selectivity. The state-of-the art system is a Co quaterpyridine adsorbed onto multiwalled carbon nanotubes, which shows exceptional selectivity (99%) at a current density up to 20 mA cm^{-2} at a 440 mV overpotential[26]. An octacyano-substituted Co phthalocyanine complex deposited onto a gas diffusion electrode (GDE) and tested in a flow cell has been reported to achieve a current density of ~30 mA cm^{-2} at an overpotential of ~550 mV with 96% selectivity for 10 h[31].

While these values represent important advances for molecular CO_2RR catalysts, much higher current densities are needed for commercial operation. Moroever, these current densities remain far below those obtained with state-of-the-art solid-state Ag[33,34] or Au[35] nanomaterials that have been reported to reach >150 mA cm^{-2}.

In this work, we design a new Co phthalocyanine (**CoPc2**) bearing one trimethyl ammonium moiety and three *tert*-butyl groups appended on the phthalocyanine macrocycle. The cobalt complex is obtained and used as a mixture of the different regioisomers, which exhibit identical electronic and steric properties[36,37], and **CoPc2** thus gives a unique electrochemical signature (Supplementary Fig. 1) with three reversible Faradaic waves that could be assigned to the Co^{II}/Co^{I} redox couple and to ligand reduction peaks[38,39]. With relatively low catalyst loadings of **CoPc2** dispersed into porous films of carbon black powder or carbon nanotubes on a carbon paper cathode, the modified electrode functions as highly effective CO_2RR electrocatalysts in acidic (pH 4), neutral (pH 7.3), and basic conditions (pH 14). Importantly, the conversion of CO_2 to CO with very high selectivities and current densities (up to 165 mA cm^{-2} at pH 14) closely matches the performances of the most active noble metal-based catalysts.

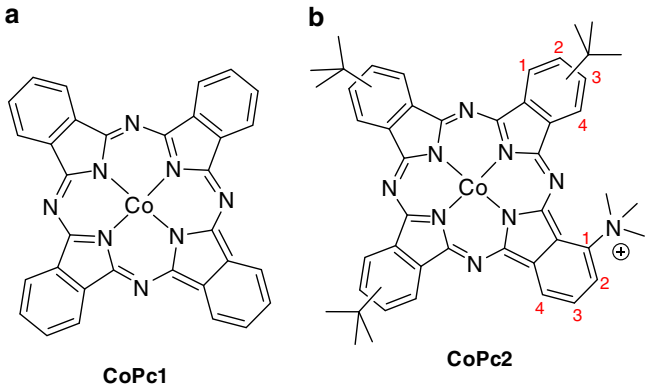

Fig. 1 Cobalt phthalocyanine catalysts **CoPc1** and **CoPc2** investigated in this study. **a CoPc1** bears no substituents. **b CoPc2** bears one trimethyl ammonium group at position 1 of the isoindole subunits, and three *tert*-butyl groups (positions 2 or 3) of the other subunits

Results

Preparation and electrochemical characterization of the catalytic inks. Cobalt complexes **CoPc1** (Fig. 1a) and **CoPc2** (Fig. 1b) were deposited onto carbon electrodes from prepared colloidal inks.

Briefly, multiwalled carbon nanotubes (MWCNTs) or carbon black were dispersed in 1:1 mixtures of EG and ethanol by sonication. The catalyst was then added to the suspension, and after sonication and addition of a small amount of Nafion®, the catalytic material was drop casted on a glassy carbon electrode ($d = 3$ mm) for cyclic voltammetry (CV) characterization, or onto carbon paper (1 or 0.5 cm^2) for preparative scale electrolysis. Typical CVs recorded in a 0.5 M $NaHCO_3$ aqueous solution (pH 7.3) are shown in Fig. 2. The reversible wave centered at ca. −0.1 V vs. RHE could be assigned to the surface confined Co^{II}/Co^{I} redox couple, as shown by the linear increase of the peak current as a function of the scan rate (Fig. 2b, e).

The electroactive amount of catalyst within the film was 1.3–1.5 nmol cm^{-2}, corresponding to about 9% of the total loaded concentration (Fig. 2e, f). Upon CO_2 saturation of the solution, the Co^{II}/Co^{I} wave remained unchanged, while a large catalytic increase of the current occurs at potentials more negative than −0.4 V vs. RHE (Fig. 2a, d). Repetitive CV shows good stability of the current response, indicative of a stable catalytic film (Supplementary Fig. 2). Remarkably, **CoPc2** gives a larger catalytic current at potentials very close from **CoPc1**, indicative of a better activity on kinetic grounds. We conjecture that the enhanced reactivity of **CoPc2** for CO_2 to CO conversion may be attributed to the through-space interactions between the positive charge of the trimethyl ammonium substituent and the partial negative charge borne by the O atoms in CO_2, which facilitate the reductive coordination of the CO_2 molecule to the Co metal center. This mechanism has been reported for a tetraphenyl Fe porphyrins substituted with same functional groups on the phenyl rings for CO_2 to CO conversion[8]. These interactions may also favor the subsequent C–O bond cleavage leading to CO formation, thus illustrating how simple tuning of the phthalocyanine substituents can accelerate the catalytic reaction. Further mechanistic studies are in preparation.

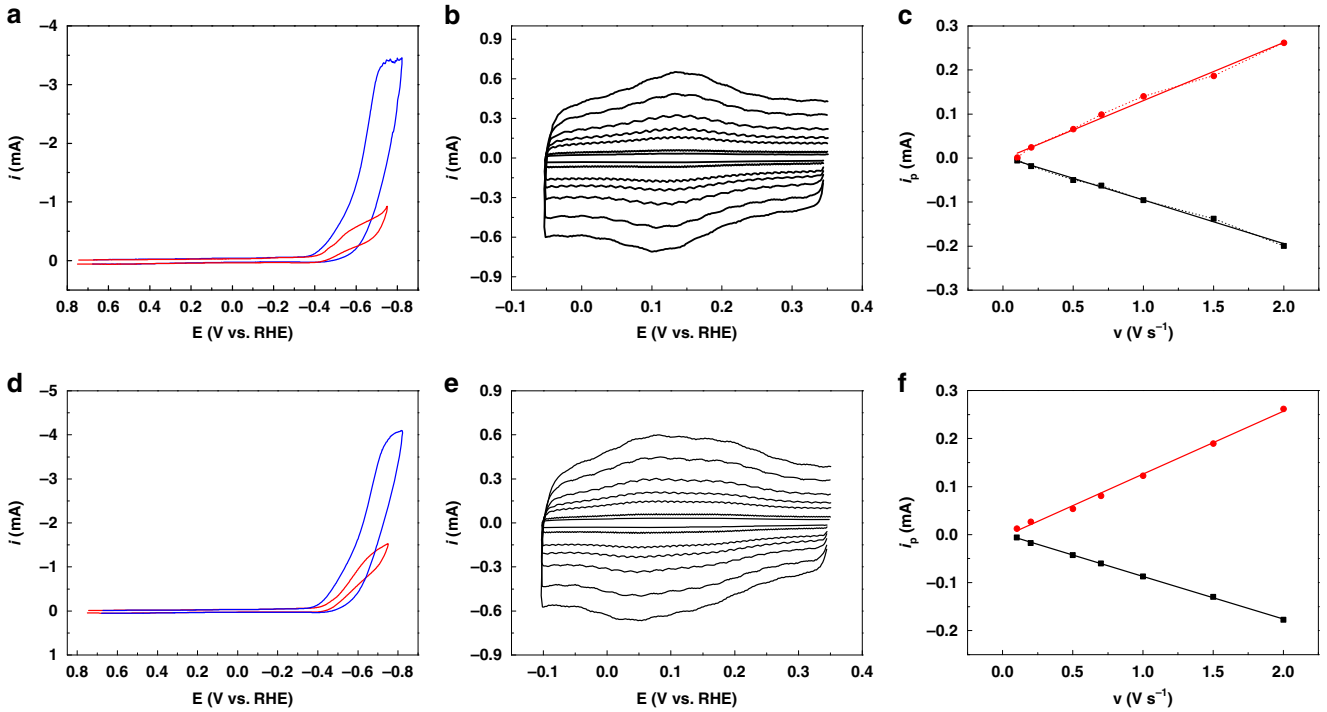

Fig. 2 Cyclic voltammetry of cobalt phthalocyanine catalytic films. Top **a**–**c** **CoPc1**@MWCNTs, bottom **d**–**f** **CoPc2**@MWCNTs. **a**, **d** CV of a cobalt phthalocyanine catalytic film deposited onto a glassy carbon electrode ($d = 3$ mm) in 0.5 M $NaHCO_3$ at $v = 0.1$ V s^{-1} under argon (red, pH 8.5) and CO_2 (blue, pH 7.3). **b**, **e** CV at various scan rates of the Co^{II}/Co^{I} wave under argon atmosphere. **c**, **f** Variation of the peak current vs. scan rate for the Co^{II}/Co^{I} redox wave. A redox active catalyst concentration of $\Gamma = 1.45 \pm 0.12$ nmol cm^{-2} was obtained from $i_p = n^2F^2vS\Gamma/4RT$ for both catalysts

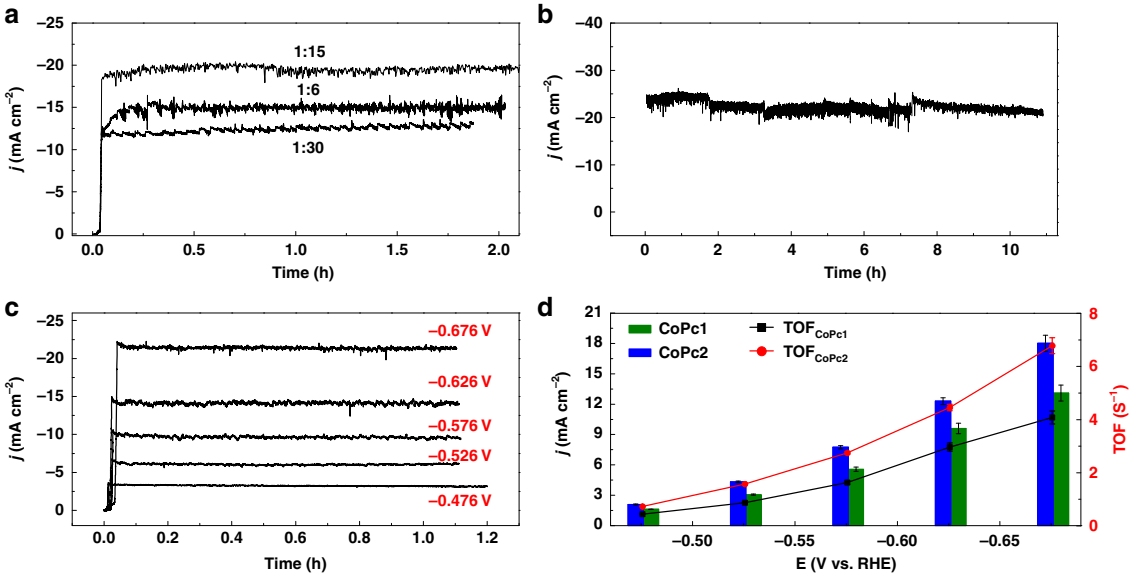

Fig. 3 Controlled potential electrolysis of CO_2 reduction. **a** Electrolysis current densities ($E = -0.676$ V vs. RHE) for a **CoPc2**@MWCNTs film at various catalyst mass ratio. **b** Long-term electrolysis ($E = -0.676$ V vs. RHE) at optimized mass ratio. **c** Variation of the current as a function of the electrolysis potential at optimized mass ratio (see text). **d** Current density and rate constant (TOF) for **CoPc1**@MWCNTs and **CoPc2**@MWCNTs for CO production in a CO_2 saturated solution containing 0.5 M $NaHCO_3$ (pH 7.3). The uncertainties represent standard errors obtained from four measurements

Electrolysis experiments at neutral and acidic pH. After the catalytic ink was deposited on a carbon paper electrode (see Methods and Supplementary Fig. 3 for a scanning electron microscopy (SEM) image of the porous catalytic film), bulk electrolysis was performed at pH neutral conditions with **CoPc2** for various loadings of the molecular catalyst. An optimal loading ratio of 1:15 (catalyst:MWCNTs weight ratio) shows reasonably good stability over the course of the 2 h experiments (Fig. 3a).

The CO selectivity was typically 92–93% in repeated runs, with H_2 being identified as a minor gas phase by-product (7–8%). No other product was detected in the liquid phase upon nuclear magnetic resonance (NMR) analysis. The electrolysis performed in the absence of catalyst or with **CoPc2**@MWCNTs (1:15) under Ar atmosphere only furnished H_2 (Supplementary Fig. 4). The TON and TOF values in Tables 1 and 2 and in the text were calculated using the total

Table 1 Comparative data for CoPc1@MWCNTs and CoPc2@MWCNTs catalytic materials during a 1 h electrolysis as a function of the potential in CO_2-saturated aqueous solution containing 0.5 M $NaHCO_3$ (pH 7.3)

E (V vs. RHE)	Entry	overpotential (mV)[a]	Catalyst[b]	j_{CO} (mA cm^{-2})[c]	TOF (CO, s^{-1})[c]	Selectivity (CO, ±0.5%)
−0.676	1	546	**CoPc1**	13.10 ± 0.79	4.08 ± 0.25	92
	2	539	**CoPc2**	18.10 ± 0.80	6.81 ± 0.30	93
−0.626	3	502	**CoPc1**	9.61 ± 0.51	2.97 ± 0.16	92
	4	498	**CoPc2**	12.3 ± 0.34	4.46 ± 0.12	92
−0.576	5	458	**CoPc1**	5.57 ± 0.21	1.63 ± 0.06	86
	6	454	**CoPc2**	7.75 ± 0.16	2.75 ± 0.06	84
−0.526	7	411	**CoPc1**	3.10 ± 0.07	0.87 ± 0.02	80
	8	410	**CoPc2**	4.33 ± 0.08	1.57 ± 0.03	73
−0.476	9	364	**CoPc1**	1.62 ± 0.01	0.44 ± 0.01	76
	10	363	**CoPc2**	2.09 ± 0.04	0.74 ± 0.01	65

[a] Corrected from ohmic drop (uncompensated solution resistance of ca. 3 Ω, electrode surface 0.5 cm^2)
[b] Γ(**CoPc1**) = 23.3 nmol cm^{-2}, Γ(**CoPc2**) = 14.4 nmol cm^{-2} (total added catalysts)
[c] The uncertainties represent standard errors obtained from four measurements

Table 2 Comparison of electrolysis performances between CoPc2@carbon powder hybrid catalyst and previously reported state-of-the art immobilized molecular Co catalysts and Ag nanomaterial

Entry	Catalyst	*E* (V vs. RHE) [overpotential (mV)]	Electrolyte	j_{CO} (mA cm^{-2})	TOF (s^{-1})	CO sel. (%)	Cell type	Ref.
1	**CoPc2**	−0.97 [836][a]	0.5 M KCl	16.3	6.1	92	H cell	this work
2	**CoPc2**	−0.676 [539][a]	0.5 M $NaHCO_3$	18.1	6.8	93	H cell	this work
3	**CoPc**	−0.676 [546][a]	0.5 M $NaHCO_3$	13.1	4.1	92	H cell	this work
4	CoPc-CN	−0.63 [520]	0.1 M $KHCO_3$	14.7	4.1	98	H cell	28
5	CoPpc	−0.61 [500]	0.5 M $NaHCO_3$	18	1.4	ca. 90	H cell	29
6	Coqpy	−0.55 [440]	0.5 M $NaHCO_3$	19.9	12	99	H cell	26
7	**CoPc2**	−0.31 [200][b]	1 M KOH	22.2	0.54	93	Flow cell	this work
8	**CoPc2**	−0.65 [540][b]	1 M KOH	70.5	1.67	94	Flow cell	this work
9	**CoPc2**	−0.72 [610][b]	1 M KOH	111.6	2.7	96	Flow cell	this work
10	**CoPc2**	−0.92 [810][b]	1 M KOH	165	3.9	94	Flow cell	this work
11	CoPc-CN	−0.66 [550]	1 M KOH	31	/	94	Flow cell	31
12	Ag[c]	−0.81 [700]	1 M KOH	156.5	/	92	Flow cell	34

Entry 1: Γ = 14.4 nmol cm^{-2} (pH 4, 2 h electrolysis), entry 2: Γ = 14.4 nmol cm^{-2} (pH 7.3, 1 h electrolysis), entry 3: Γ = 23.3 nmol cm^{-2} (pH 7.3, 1 h electrolysis), entries 7–10: Γ = 0.216 μmol cm^{-2} (pH 14, for 0.5, 10, 3, and 0.3 h electrolysis, respectively).
[a] Corrected from ohmic drop (uncompensated solution resistance of ca. 3 Ω, electrode surface 0.5 cm^2)
[b] Uncorrected from ohmic drop
[c] Carbonate-derived Ag nano-catalyst (500 nm thickness), see Ref. [34] for details

amount of catalyst added in the films, hence these values are underestimated.

Using this 1:15 catalyst loading weight ratio, the effect of the applied potential on efficiency and selectivity was investigated for both the cobalt catalysts at pH neutral conditions (Fig. 3c and Supplementary Fig. 5). As shown in Fig. 3d, the current density was systematically larger for **CoPc2** as compared to **CoPc1** (ca. 25% increase). Concomitantly, the CO selectivity increases at more negative electrolysis potentials, with a relative higher increase for **CoPc2** (Table 1). This shows that, at more negative potentials, the catalytic CO_2 reduction reaction outruns the H_2 evolution reaction. At −0.676 V vs. RHE which corresponds to an overpotential η = 546 mV and in neutral pH conditions, **CoPc1** gave 92% CO with an average partial current density of 13.1 mA cm^{-2} (Table 1, entry 1). At the same potential (η = 539 mV), a 1 h electrolysis with **CoPc2** led to a TON of 24516 for CO (TOF = 6.8 s^{-1}) with 93% selectivity. The partial current density for CO production reaches 18.1 mA cm^{-2} (Table 1, entry 2).

Longer term electrolysis at pH 7.3 further demonstrates the excellent stability of the catalytic system, since no decrease in either the current density or the selectivity for CO production were observed upon a 10.5 h experiment. An average selectivity of 91% for CO production along with j_{CO} close to 20 mA cm^{-2} (Fig. 3b) were measured. XPS analysis of the cathode material before and after electrolysis does not reveal major changes of the Co 2p and N 1 s peaks, suggesting integrity of the molecular catalyst during the entire course of the electrolysis (Supplementary Fig. 6). Remarkably, an electrolysis (2 h) at E = − 0.971 V vs. RHE in a CO_2 saturated 0.5 M KCl solution (pH 4) led to equally good results, with a selectivity of 92% and j_{CO} = 17 mA cm^{-2} (Supplementary Fig. 7). When the cobalt phtalocyanine bearing four t-butyl groups (**4-Co**) was used as catalyst in an electrolysis experiment (1:15 catalyst loading weight ratio, E = −0.676 V vs. RHE) in neutral pH conditions, a Faradaic efficiency of 92% for CO was obtained with an average CO partial current density of 15.8 mA cm^{-2} (Supplementary Fig. 8). This reference complex is thus less active than **CoPc2**, further illustrating that the enhanced activity of **CoPc2** may arise from the trimethyl ammonium substituent on the ligand via through-space effects.

Electrolysis experiments in basic solutions using a flow cell. Encouraged by these results, we included **CoPc2** into a flow cell setup comprising **CoPc2** supported on a GDE as the cathode, in order to realize CO_2 to CO conversion in industrial setting.

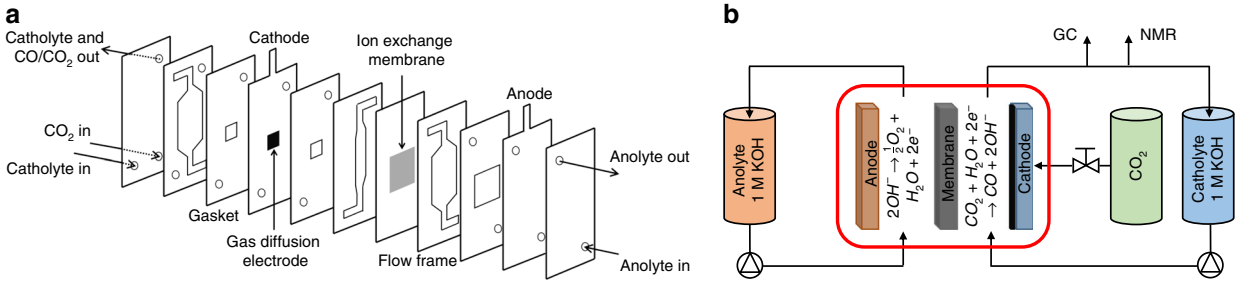

Fig. 4 Graphic illustration of the CO_2 electrolyzer flow cell. **a** Cross-sectional view of the cell and **b** general scheme of the entire experimental set-up

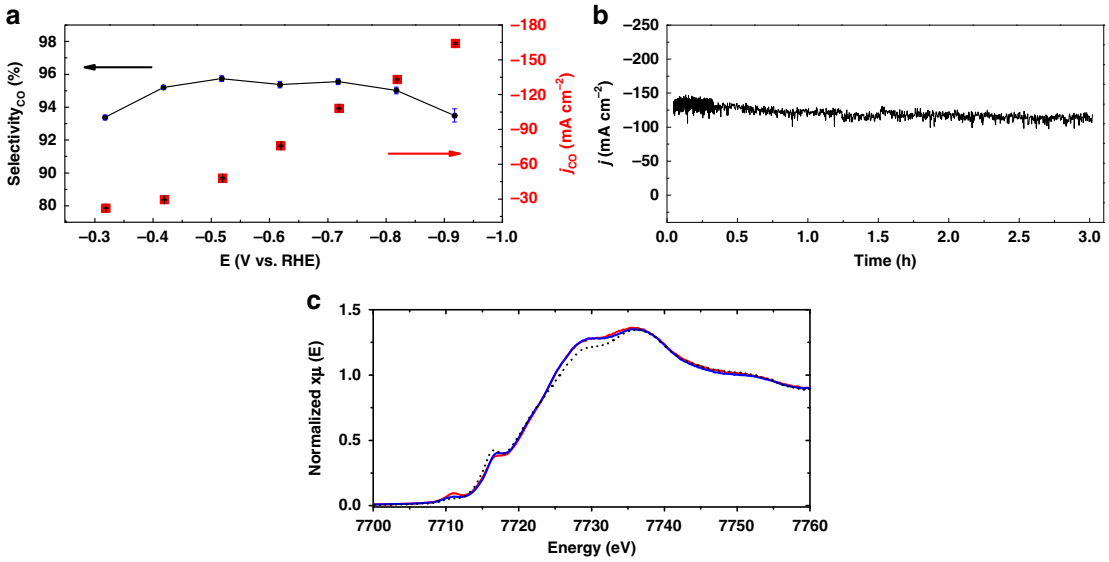

Fig. 5 Controlled potential electrolysis and **CoPc2** film characterization. **a** Current density and selectivity for CO production as a function of the potential and **b** bulk electrolysis at fixed potential ($E = -0.72$ V vs. RHE) for **CoPc2**@carbon black deposited onto a carbon paper as cathodic material, in 1 M KOH. **c** Co K-edge XANES profiles of CoPc2 (black dots) and **CoPc2**@carbon black before (blue) and after electrolysis ($E = -0.72$ V vs. RHE) (red) in 1 M KOH solution

Details of the setup are provided in the methods. Briefly, the electrolyzer consists of a sandwich of flow frames, electrodes, gaskets and an ion exchange membrane, which were assembled as schematically illustrated in Fig. 4a. A gas flow of CO_2 is delivered from the back side of the cathodic compartment and flows through the GDE, while the catholyte solution is circulated in between the GDE and the anion exchange membrane (AEM). On the other side of the AEM, the anolyte is directed between the AEM and the Pt/Ti alloy anode, Fig. 4b. **CoPc2** was dispersed in a colloidal ink with carbon black and subsequently deposited on the carbon fiber paper, composing the cathode.

At −0.3 V vs. RHE, which corresponds to a low 200 mV overpotential, a high current density with $j_{CO} = 22.2$ mA cm^{-2} was achieved. The dependence of the current density for CO production is reported in Fig. 5a (see also Supplementary Fig. 9). Upon setting the electrolysis potential at −0.72 V vs. RHE, j_{CO} raised to 111.6 mA cm^{-2} with 96% selectivity, while excellent stability over the course of the 3 h electrolysis was obtained (Fig. 5b). The only additional gas phase by-product was H_2 (4% selectivity) and the catholyte solution was carefully checked by ^{1}H NMR. Formate or methanol were not detected while the absence of any **CoPc2** trace further indicate that the molecular catalyst is not leaching out of the supporting film. The obtained j_{CO} corresponds to a turnover frequency (TOF) of 2.7 s^{-1} and a turnover number (TON) of 29,008. A maximum current density of 165 mA cm^{-2} for CO generation was obtained at −0.92 V vs. RHE. Long-term stability of the catalytic material was further illustrated upon applying a constant current density of 75 mA cm^{-2} for 10 h, which led to a cathodic potential of −0.65 V vs. RHE ($\eta = 540$ mV) with 94% selectivity of CO ($j_{CO} = 70.5$ mA cm^{-2}) (Supplementary Fig. 10). All the collected data are compiled in Table 2, along with a comparison of previously reported catalysts. The type of cell used (H cell vs. flow cell) is also indicated to ease comparison between data. The Co K-edge XANES spectra of **CoPc2**@carbon black were recorded before and after electrocatalysis at $E = -0.72$ V vs. RHE. Figure 5c shows these spectra together with that of the starting **CoPc2** complex. All these spectra present the typical features expected for a cobalt (II) phthalocyanine complex, i.e., a low intensity pre-edge peak at 7711 eV (corresponding to a 1s to 3d/4p transition) and a shoulder at 7717 eV (corresponding to a 1s to 4p$_z$ transition)[29,40,41]. The intensity of these two transitions were shown by Li et al.[41] to depend on the attachment to a surface, i.e., the pre-edge intensity increases and the shoulder decreases upon adsorption onto nanotubes, respectively.

The same trend is observed in the **CoPc2**@carbon black system, with decreased pre-edge and increased shoulder intensities on going from the starting complex to the adsorbed species. This trend retains after catalysis, suggesting an even closer interaction with the surface while maintaining the overall

structure of the molecular catalyst after the experiment. This conservation of structure is further confirmed by the EXAFS spectra (Supplementary Fig. 11), which also present the typical features of a cobalt phthalocyanine complex[41]. In addition, comparison of the spectrum of **CoPc2**@carbon black recorded after catalysis with those of reference cobalt samples (Supplementary Fig. 11) clearly shows that the changes observed on the spectrum after catalysis are insignificant as far as the overall structure is concerned.

Discussion

Remarkably, **CoPc2** remains highly selective for the CO_2-to-CO conversion across 10 pH units, extending from acidic (pH 4) to basic solutions (pH 14). An averaged 92% selectivity for CO_2 reduction with partial current densities of ca. 20 mA cm^{-2} were routinely obtained in the whole domain of pH values with excellent stability over time. In close to neutral solutions (pH 7.3), **CoPc2** is a significantly better catalyst than the nonsubstituted phthalocyanine **CoPc1** (see Table 2, entries 2 and 3) with a ca. 25% increase in current density at similar overpotential, but it also surpasses state-of-the art tetra-cyano substituted phthalocyanine (CoPc-CN, Table 2, entry 4) and unsubstituted Co phthalocyanine polymerized around carbon nanotubes (CoPpc, Table 2, entry 5), both in terms of current density and TOF. Similarly to the previously reported cobalt phthalocyanines mentioned above, **CoPc2** exhibits excellent stability over time, as illustrated in Fig. 3b, showing a 10.5 h electrolysis experiment, with no loss of performance. A TOF up to 6.8 s^{-1} was reached and, generally, only a very small loading of the catalysts was necessary to obtain high j_{CO} (see for example Table 2, entries 1–2). In a 1 M KOH electrolyte solution (pH 14), ca. 20 mA cm^{-2} could be obtained at a very low overpotential of 200 mV, once the hybrid catalyst mixed with carbon support was included in a gas flow cell (Table 2, entry 7). Long-term electrolysis (10 h) in basic conditions (pH 14) at −0.65 V vs. RHE led to an average j_{CO} close to 70.5 mA cm^{-2}. The ability to implement **CoPc2** in various pH conditions is also a key feature that may allow for combining the Co catalyst to various types of anodic materials in order to decrease the overall cell potential. In particular, the excellent performance obtained at pH 14 could permit pairing of the **CoPc2** loaded cathode with the most efficient oxygen evolving metal oxide anode materials. At this pH, at −0.92 V vs. RHE, this hybrid catalyst can form CO with 94% selectivity at a partial current density of 165 mA cm^{-2}, matching the state-of-the art Ag based catalyst sputtered onto a PTFE membrane, both in terms of selectivity and current density (Table 2, compare entries 10 and 12).

In conclusion, upon introducing a positively charged trimethyl ammonium group and three tert-butyl groups on the parent cobalt phthalocyanine, a highly efficient and versatile catalyst for the CO_2-to-CO electrochemical conversion in water has been obtained. This study highlights that rational tuning of the structure of simple metal complexes may allow for high CO_2 electroreduction performances, and it is likely that further improvement is yet to come. This work opens up new perspectives for the development of low-cost catalytic materials to be included in CO_2 electrolyzers that will hopefully soon emerge at an industrial scale.

Methods

Chemicals. Chemicals and materials were purchased from Sigma-Aldrich, Fluka, TCI America, ABCR or Alfa Aesar, and used as received. All aqueous solutions were prepared with Millipore water (18.2 MΩ cm). The MWCNTs were purchased from Sigma-Aldrich (O.D. × L 6–9 nm × 5 µm, >95%). The cobalt (II) phthalocyanine (**CoPc1**) (β-form, dye content 97%) was purchased from Sigma-Aldrich. Toray Carbon Paper (CAS number: 7782-42-5), TGP-H-60, 19 × 19 cm was purchased from Alfa Aesar and used for preparation of the cathodes for the electrochemical cell. The cathodes (GDEs) used in the flow cell were prepared using Freudenberg C24H5 carbon paper (21 × 29.7 cm, product code F5GDL). VULCAN® XC72R Speciality Carbon Black was purchased from Cabot Corporation. 4-*Tert*-butylphthalonitrile was obtained from TCI America. 3-Nitrophthalonitrile was purchased from ABCR. All solvents were of synthetic grade. Supplementary Fig. 13 describes the synthesis and characterization of **CoPc2**, and supplementary Figs. 14–27 provide characterization of reaction intermediates and final compound.

Preparation of the hybrid materials. For CV experiments and electrolysis in the closed electrolysis cell, 3 mg of MWCNTs were dispersed in 2 mL ethylene glycol (EG)/ethanol (EtOH) 1:1(v/v) mixture followed by 30 min of sonication. Totally, 1 mg of the cobalt catalyst (**CoPc1**, **CoPc2**) was dissolved in 1 mL EG/EtOH mixture. Various volumes of this solution were added to the MWCNTs suspension in a total volume of 3 mL, so as to get mass ratio (1:6, 1:15 and 1:30) of the catalyst. The suspension was further sonicated for 30 min. Finally, Nafion® was added (2.9 %, 30 µL) and the complete mixture was sonicated for 30 min to obtain the final catalytic ink.

For the flow cell set-up, 3 mg of carbon black were dispersed in 3 mL EtOH followed by 30 min of sonication. Totally, 0.2 mg of **CoPc2** was dissolved in 1 mL EtOH so as to get a mass ratio (1:15) of the catalyst. The suspension was further sonicated for 30 min. Finally, Nafion® was added (2.9%, 30 µL) and the complete mixture was sonicated for 30 min to obtain the final catalytic ink. The ink was drop casted on carbon paper masked with a Teflon frame to obtain an electrode area of 1 × 1 cm^2.

Electrochemical studies. CV experiments were performed using an AUTOLAB PGSTAT128N potentiostat (Metrohm). Controlled potential electrolysis were performed using a PARSTAT 4000A potentiostat (Princeton Applied Research).

CV: The three-electrode setup consisted of a glassy carbon working electrode (custom made, 0.071 cm^2), a Pt wire counter electrode, and a SCE reference electrode (−0.241 V vs. NHE). The working electrode was polished with diamond paste (15, 6, 3, and 1 µm successively, 60 s per polishing cycle), thoroughly rinsed and sonicated in ethanol, and dried. Totally, 10 µL of the hybrid materials suspension were dropped on the surface of the electrode, and allowed to dry under 100 °C ambient conditions. Ohmic drop was compensated using the positive feedback compensation implemented in the instrument.

Preparative scale electrolysis: In the closed cell, experiments were carried out in a cell using a Toray carbon paper as working electrode, and a SCE reference electrode closely positioned one from the other. The Pt grid counter electrode was separated from the cathodic compartment with a glass frit. The catalytic ink was dropped on one face of the Toray carbon paper cathode (100 µL for a 0.5 cm^2 electrode), and allowed to dry under 100 °C ambient conditions prior to use. The full cell setup was identical to the one used previously[26].

The flow cell electrolyzer (Micro Flow Cell® purchased by Electrocell) is composed by a sandwich of flow frames, electrodes, gaskets, and a membrane, which, when assembled as illustrated in Fig. 3, constitute a three-compartment flow cell. One compartment delivers the CO_2 (at 16.7 sccm) from the back side and through the GDE (1 × 1 cm^2, fixated in a Ti frame), while another directs the catholyte solution (1 M KOH, flow rate of 16 sccm) in between the GDE and the AEM (Sustainion™ X37-50). On the other side of the latter, the anolyte (1 M KOH, flow rate of 16 sccm) is directed between the AEM and the Pt/Ti alloy anode. The flow frames are made of PTFE, and the gaskets of peroxide cured EDPM. Catholyte and anolyte were recycled using peristaltic pumps. All tubings were made of PTFE and connected to the cell with PEEK ferrules and fittings. The whole setup is schematically shown Supplementary Fig. 12.

Gas detection. Gas chromatography analyses of gas sampled from the headspace during the electrolysis were performed with an Agilent Technologies 7820A GC system equipped with a thermal conductivity detector. CO and H_2 production was quantitatively detected using a CP-CarboPlot P7 capillary column (27.46 m in length and 25 µm internal diameter). Temperature was held at 150 °C for the detector and 34 °C for the oven. The carrier gas was argon flowing at 9.5 mL/min at constant pressure of 0.4 bars. Injection was performed via a 250-µL gas-tight (Hamilton) syringe previously degassed with CO_2. Conditions allowed detection of both H_2, O_2, N_2, CO, and CO_2. Calibration curves for H_2 and CO were determined separately by injecting known quantities of pure gas.

Material characterizations. An X-Ray Photoelectron Spectrometer THERMO-VG ESCALAB 250 (RX source K AI (1486.6 eV)) was used. X-ray absorption spectra were collected at the LUCIA beamline of SOLEIL with a ring energy of 2.75 GeV and a current of 490 mA. The energy was monochromatized by means of a Si (111) double crystal monochromator. Data were collected in a primary vacuum chamber as fluorescence spectra with an outgoing angle of 5° using a Bruker silicon drift detector. The data were normalized to the intensity of the incoming incident energy and processed with the Athena software from the IFEFFIT package. For the EXAFS analysis, an E_0 value of 7715.4 eV was used for the cobalt K-edge jump energy. SEM using a field emission gun was performed using a Zeiss Supra 40. Infrared spectra (IR) were recorded on a Bio-Rad FTS 175 C Fourier transform infrared spectrometer spectrophotometer. Ultraviolet (UV)–visible absorption

spectra were obtained using a Shimadzu 2001 UV spectrophotometer. High resolution mass spectra were measured on an Agilent 6530 Accurate-Mass Q-TOF LC/MS spectrometer equipped with electrospray ionization source. NMR spectra were recorded in deuterated chloroform ($CDCl_3$) and THF-d_8 on a Varian 500 MHz spectrometer. Melting points were recorded on a Stuart SMP apparatus.

Data availability

Data supporting the findings of this study are available within the Article and its Supplementary Information, or from the corresponding authors upon reasonable request.

Received: 22 February 2019 Accepted: 19 July 2019
Published online: 09 August 2019

References

1. Aresta, M., Dibenedetto, A. & Angelini, A. Catalysis for the valorization of exhaust carbon: from CO_2 to chemicals, materials, and fuels. technological use of CO_2. *Chem. Rev.* **114**, 1709–1742 (2014).
2. Jhong, H.-R. M., Ma, S. & Kenis, P. J. A. Electrochemical conversion of CO_2 to useful chemicals: current status, remaining challenges, and future opportunities. *Curr. Opin. Chem. Eng.* **2**, 191–199 (2013).
3. Seh, Z. W. et al. Combining theory and experiment in electrocatalysis: Insights into materials design. *Science* **355**, eaad4998 (2017).
4. Costentin, C., Robert, M. & Savéant, J.-M. Catalysis of the electrochemical reduction of carbon dioxide. *Chem. Soc. Rev.* **42**, 2423–2436 (2013).
5. Qiao, J., Liu, Y., Hong, F. & Zhang, J. A review of catalysts for the electroreduction of carbon dioxide to produce low-carbon fuels. *Chem. Soc. Rev.* **43**, 631–675 (2014).
6. Elgrishi, N., Chambers, M. B., Wang, X. & Fontecave, M. Molecular polypyridine-based metal complexes as catalysts for the reduction of CO_2. *Chem. Soc. Rev.* **46**, 761–796 (2017).
7. Grice, K. A. Carbon dioxide reduction with homogenous early transition metal complexes: opportunities and challenges for developing CO_2 catalysis. *Coord. Chem. Rev.* **336**, 78–95 (2017).
8. Azcarate, I., Costentin, C., Robert, M. & Savéant, J.-M. Through-space charge interaction substituent effects in molecular catalysis leading to the design of the most efficient catalyst of CO_2-to-CO electrochemical conversion. *J. Am. Chem. Soc.* **138**, 16639–16644 (2016).
9. Francke, R., Schille, B. & Roemelt, M. Homogeneously catalyzed electroreduction of carbon dioxide—methods, mechanisms, and catalysts. *Chem. Rev.* **116**, 4631–4701 (2018).
10. Grills, D. C., Ertem, M. Z., McKinnon, M., Ngo, K. T. & Rochford, J. Mechanistic aspects of CO_2 reduction catalysis with manganese-based molecular catalysts. *Coord. Chem. Rev.* **374**, 173–217 (2018).
11. Loewen, N. D., Neelakantan, T. V. & Berben, L. A. Renewable formate from C–H bond formation with CO_2: using iron carbonyl clusters as electrocatalysts. *Acc. Chem. Res.* **50**, 2362–2370 (2017).
12. Takeda, H., Cometto, C., Ishitani, O. & Robert, M. Electrons, photons, protons and earth abundant metal complexes for molecular catalysis of CO_2 reduction. *ACS Catal.* **7**, 70–88 (2017).
13. Shen, J. et al. Electrocatalytic reduction of carbon dioxide to carbon monoxide and methane at an immobilized cobalt protoporphyrin. *Nat. Commun.* **6**, 8177 (2015).
14. Rao, H., Schmidt, L. C., Bonin, J. & Robert, M. Visible-light-driven methane formation from CO_2 with an iron complex. *Nature* **548**, 74–77 (2017).
15. Rao, H., Lim, C.-H., Bonin, J., Miyake, G. M. & Robert, M. Visible-light-driven conversion of CO_2 to CH_4 with an organic sensitizer and an iron porphyrin catalyst. *J. Am. Chem. Soc.* **140**, 17830–17834 (2018).
16. Tatin, A. et al. Efficient electrolyser for CO_2 splitting in neutral water using earth abundant materials. *Proc. Natl Acad. Sci. USA* **113**, 5526–5529 (2016).
17. Maurin, A. & Robert, M. Noncovalent immobilization of a molecular iron based electrocatalyst on carbon electrodes for selective, efficient CO_2-to-CO conversion in water. *J. Am. Chem. Soc.* **138**, 2492–2495 (2016).
18. Mohamed, E. A., Zahran, Z. N. & Naruta, Y. Efficient heterogeneous CO_2 to CO conversion with a phosphonic acid fabricated cofacial iron porphyrin dimer. *Chem. Mater.* **29**, 7140–7150 (2017).
19. Choi, J. et al. A porphyrin/graphene framework: a highly efficient and robust electrocatalyst for carbon dioxide reduction. *Adv. Energy Mater.* **8**, 1801280 (2018).
20. Choi, J. et al. Energy efficient electrochemical reduction of CO_2 to CO using a three-dimensional porphyrin/graphene hydrogel. *Energy Environ. Sci.* **12**, 747–755 (2019).
21. Sonoyama, N., Kirii, M. & Sakata, T. Electrochemical reduction of CO_2 at metal-porphyrin supported gas diffusion electrodes under high pressure CO_2. *Electrochem. Commun.* **1**, 213–216 (1999).
22. Aoi, S., Mase, K., Ohkubo, K. & Fukuzumi, S. Selective electrochemical reduction of CO_2 to CO with a cobalt chlorin complex adsorbed on multi-walled carbon nanotubes in water. *Chem. Commun.* **50**, 10226–10228 (2015).
23. Hu, X.-M., Ronne, M. H., Pedersen, S. U., Skrydstrup, T. & Daasbjerg, K. Enhanced catalytic activity of cobalt porphyrin in CO_2 electroreduction upon immobilization on carbon materials. *Angew. Chem. Int. Ed.* **56**, 6468–6472 (2017).
24. Rotundo, L. et al. Electrochemical CO_2 reduction in water at carbon cloth electrodes functionalized with a fac-Mn (apbpy)$(CO)_3$Br complex. *Chem. Commun.* **55**, 775–777 (2019).
25. Walsh, J. J., Neri, G., Smith, C. L. & Cowan, A. J. Electrocatalytic CO_2 reduction with a membrane supported manganese catalyst in aqueous solution. *Chem. Commun.* **50**, 12698–12701 (2014).
26. Wang, M., Chen, L., Lau, T.-C. & Robert, M. Hybrid Co quaterpyridine complex/carbon nanotube catalytic material for CO_2 reduction in water. *Angew. Chem. Int. Ed.* **57**, 7769–7773 (2018).
27. Morlanes, N., Takanabe, K. & Rodionov, V. Simultaneous reduction of CO_2 and splitting of H2O by a single immobilized cobalt phthalocyanine electrocatalyst. *ACS Catal.* **6**, 3092–3095 (2016).
28. Zhang, X. et al. Highly selective and active CO_2 reduction electrocatalysts based on cobalt phthalocyanine/carbon nanotube hybrid structures. *Nat. Commun.* **8**, 14675 (2017).
29. Han, N. et al. Supported cobalt phthalocyanine for high-performance electrocatalytic CO_2 reduction. *Chem* **3**, 652–664 (2017).
30. Chen, C. et al. Enhanced CO_2 electroreduction via interaction of dangling S bonds and Co sites in cobalt phthalocyanine/$ZnIn_2S_4$ hybrids. *Chem. Sci.* **10**, 1659–1663 (2019).
31. Xu, L. et al. High-performance electrochemical CO_2 reduction cells based on non-noble metal catalysts. *ACS Energy Lett.* **3**, 2527–2532 (2018).
32. Choi, J. et al. Steric modification of a cobalt phthalocyanine/graphene catalyst to give enhanced and stable electrochemical CO_2 reduction to CO. *ACS Energy Lett.* **4**, 666–672 (2019).
33. Kutz, R. B. et al. Sustainion imidazolium-functionalized polymers for carbon dioxide electrolysis. *Energy Technol.* **5**, 929–936 (2017).
34. Dinh, C.-T., García de, ArquerF. P., Sinton, D. & Sargent, E. H. High rate, selective, and stable electroreduction of CO_2 to CO in basic and neutral media. *ACS Energy Lett.* **3**, 2835–2840 (2018).
35. Verma, S. et al. Insights into the low overpotential electroreduction of CO_2 to CO on a supported gold catalyst in an alkaline flow electrolyzer. *ACS Energy Lett.* **3**, 193–198 (2018).
36. Li, X. et al. Nanostructured phthalocyanine assemblies with protein-driven switchable photoactivities for biophotonic imaging and therapy. *J. Am. Chem. Soc.* **139**, 10880–10886 (2017).
37. Cao, J. et al. Efficient grain boundary suture by low-cost tetra-ammonium zinc phthalocyanine for stable perovskite solar cells with expanded photoresponse. *J. Am. Chem. Soc.* **140**, 11577–11580 (2018).
38. Manbeck, G. F. & Fujita, E. A review of iron and cobalt porphyrins, phthalocyanines and related complexes for electrochemical and photochemical reduction of carbon dioxide. *J. Porphyr. Phthalocyanines* **19** (01n03), 45–64 (2015).
39. Akyüz, D., Keleş, T., Biyiklioglu, Z. & Koca, A. Metallophthalocyanines bearing polymerizable {[5-({(1E)-[4-(diethylamino) phenyl] methylene} amino)-1-naphthy1] oxy} groups as electrochemical pesticide sensor. *Electroanalysis* **29**, 2913–2924 (2017).
40. Dodelet, J. P. Oxygen reduction in PEM fuel cell conditions: heat-treated non-precious metal-N4 macrocyles and beyond. In (eds Zagal J. H., Bedioui F. & Dodelet J. P.) N4-Macrocyclic Metal Complexes. Ch. 3. 91–99 (Springer, 2006).
41. Li, N., Lu, W., Pei, K. & Chen, W. Interfacial peroxidase-like catalytic activity of surface-immobilized cobalt phthalocyanine on multiwall carbon nanotubes. *RSC Adv.* **5**, 9374–9380 (2015).

Acknowledgements

M.W. thanks the China Scholarship Council for her PhD fellowship (CSC student number 201606220034). SOLEIL and the MiChem LABEX (Sorbonne Université) are acknowledged for a PhD fellowship to D.M. Partial financial support to M.R. from Air Liquide and from the Institut Universitaire de France (IUF) are also gratefully acknowledged.

Author contributions

U.I., M.R. and C.P.B. designed and supervised the project. U.I. and F.D. synthesized and characterized the catalysts. M.W., K.T., D.S., D.J. and S.R. carried out the CO_2 reduction experiments and analyzed the data. D.M. and B.L.-K. performed and analyzed the XAS experiments. All authors discussed the results and assisted during paper preparation.

Additional information

Supplementary Information accompanies this paper at https://doi.org/10.1038/s41467-019-11542-w.

Competing interests: The authors declare no competing interests.

Reprints and permission information is available online at http://npg.nature.com/reprintsandpermissions/

Peer review information: *Nature Communications* would like to thank Kyle Grice and other, anonymous, reviewers for their contributions to the peer review of this work.

Publisher's note: Springer Nature remains neutral with regard to jurisdictional claims in published maps and institutional affiliations.

Open Access This article is licensed under a Creative Commons Attribution 4.0 International License, which permits use, sharing, adaptation, distribution and reproduction in any medium or format, as long as you give appropriate credit to the original author(s) and the source, provide a link to the Creative Commons license, and indicate if changes were made. The images or other third party material in this article are included in the article's Creative Commons license, unless indicated otherwise in a credit line to the material. If material is not included in the article's Creative Commons license and your intended use is not permitted by statutory regulation or exceeds the permitted use, you will need to obtain permission directly from the copyright holder. To view a copy of this license, visit http://creativecommons.org/licenses/by/4.0/.

© The Author(s) 2019